TiO 2 nanomaterial detection in calcium rich matrices by spICPMS. A matter of resolution and treatment

Mickaël Tharaud, Andreas Gondikas, Marc F. Benedetti, Frank von der Kammer, Thilo Hofmann, Geert Cornelis

TiO_2 nanomaterials detection in calcium rich matrices by spICPMS.

A matter of resolution and treatment.

Mickael Tharaud*, Andreas P. Gondikas[§ß], Marc F. Benedetti*, Frank von der Kammer[§], Thilo Hofmann[§], Geert Cornelis[†].

*Institut de Physique du Globe de Paris, Sorbonne Paris Cité, Univ Paris Diderot, CNRS, F-75005 Paris, France.
[§]University of Vienna, Department of Environmental Geosciences and Environmental Science Research Network, Althanstr. 14, UZA II, 1090 Vienna, Austria.
[ß]Department of Marine Sciences, University of Gothenburg, Kristineberg 566, 45178 Fiskebäckskil, Sweden
[†]Swedish University of Agricultural Sciences, Uppsala, Sweden.

Corresponding author
*e-mail: tharaud@ipgp.fr
tel.:+33-1-83-95-78-78
fax: +33-1-83-95-77-08

Notes
The authors declare no competing financial interest.

Abstract

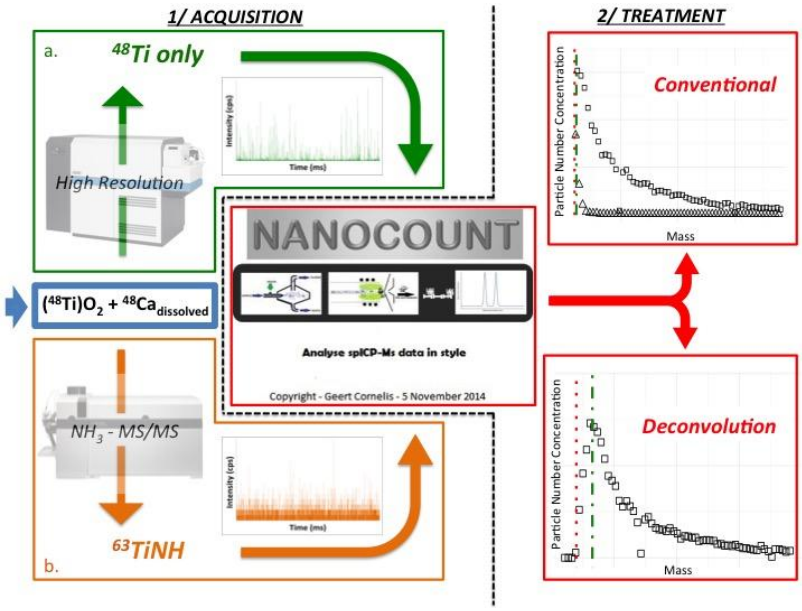

High Ca concentrations in complex matrices such as river waters often hamper detection of titanium nanomaterials (TiO_2 NPs) by single particle inductively coupled plasma mass spectrometry (spICPMS), because of isobaric interferences of ^{48}Ca on the most abundant Ti isotope (^{48}Ti). Several approaches were used to reduce this interference while measuring TiO_2 in solutions with different Ca concentrations up to 100 mg L^{-1}. ICP-MS/MS was used with ammonia as reaction cell gas and high resolution (HR) ICP-MS was used at different resolution settings. These approaches were compared with measuring different Ti isotopes (^{47}Ti, ^{49}Ti). spICPMS data was then treated with a deconvolution method to filter out dissolved signals and identify the best approach to detect the lowest possible corresponding spherical size of TiO_2 NP (D_{min}). ICP-MS/MS allowed for an

important decrease of the theoretical D_{min} compared to standard quadrupole ICP-MS, down to 64 nm in ultrapure water, however the sensitivity was reduced by the reaction gas and increasing Ca concentrations also increased the $D_{min.}$ The comparably higher sensitivity of HR-ICP-MS allowed for theoretically measuring D_{min} of 10 nm in ultrapure water. Combined with the deconvolution analysis, the highest resolution mode in HR-ICP-MS leads to the lowest D_{min} at high Ca concentrations, even though significant broadening of the measured mass distributions occurred for TiO_2 NPs at Ca concentrations up to 100 mg L^{-1}.

Acknowledgments

The authors would like to acknowledge the support provided by the European COST action ES1205, Engineered Nanomaterials - From Wastewater Treatment & Stormwater to Rivers (ENTER). Geert Cornelis would like to acknowledge funding from the Swedish research council (VR project C0393701). Part of this work was supported by IPGP multidisciplinary program PARI, and by Region île-de-France SESAME Grant no. 12015908.

Introduction

Titanium based nanomaterials (TiO_2 NPs) have properties for many applications such as cosmetic products, medication, pigments [1]. More than 50,000 tons of these materials were produced in 2010, a value expected to rise to 201,000 tons by 2015 and thus, becoming one of the most produced NPs in the world [2]. The fate, behaviour and potential toxicity of TiO_2 NPs after being released in the environment are under debate [3]. It was shown for NPs other than TiO_2, that relatively smaller NPs potentially exert more toxicity than larger ones because of a higher bioavailability [4]. There is thus a need to develop methods of detection for relatively small TiO_2 NPs, both from a risk assessment point of view and quality control in production.

Most of the common techniques used for determination of particle number concentration, size and composition present several limitations such as extensive time investment (*i.e.* transmission electron microscopy), limitations with regards to lowest detectable size and number concentration (nanoparticle tracking analysis) and the impossibility to analyse number concentrations of polydisperse suspensions (dynamic light scattering) [5 6]. Moreover, the principal weakness of all these methods is the impossibility to determine all 3 parameters simultaneously [7]. Thus, using the rapidity, selectivity and sensitivity of inductively coupled plasma mass spectrometry (ICP-MS), single particle ICP-MS (spICPMS) is becoming a powerful technique for the simultaneous determination of the number concentration, the size and the composition of NPs [8]. Indeed, this

technique allows a precise and rapid detection of NPs without much sample treatment [9] in complex environmental samples where low NP concentration and high dissolved concentrations can be found [10].

The concept of spICPMS is well explained by Degueldre *et al.* [11]. Briefly, a solution containing NPs is nebulized into the plasma. NPs form an ion cloud that is sampled by the mass spectrometer and finally collected by the detector. At millisecond dwell times, the ion cloud produces a signal pulse, whose intensity is directly proportional to the number of ions in the cloud and therefore to the NP size, if the particle shape, density and composition are known. As these are often not completely known, a spherical size and a particular composition (e.g. TiO_2) are usually assumed leading to a metric that can be described as the corresponding spherical size, which will shortly be referred to as "size" in this work. An external calibration (intensity vs mass) using corresponding dissolved metal standards of known concentration is necessary. First, the intensity of the pulse is converted to mass using the slope, the y-intercept and the transmission efficiency and, supposing a spherical shape, a size is determined. Then, assuming a constant nebulisation efficiency, the number of detected pulses is directly proportional to the particle number concentration in the sample [12]. Note that, the transmission efficiency equals the proportion of ions generated in the plasma that is eventually detected and the nebulisation (*i.e.* transport) efficiency is the ratio of the number of NPs that enter the plasma to the total number aspirated. Both are calculated using Au NPs as reference NPs.

The two major challenges of spICPMS for the purpose of determining particle sizes are the measurement of particles whose size is close to the limit of detection (D_{min}) and the assumptions that have to be made in terms of particle shape and composition. In spICPMS two detection limits are of importance: the D_{min} which is the lowest detectable particle size and ($LOD_{numberconcentration}$) which is the lowest detectable particle number concentration above background particle counts and shot noise and must not be confused with detection limits of ICP-MS for detection of dissolved ions (LOD_{ion}). This work focuses on D_{min}, *i.e.* the lowest NP size calculated from the lowest intensity distinguishable from the background and the associated noise. D_{min} is influenced by the composition and stoichiometry of the particle and eventually the isotope measured and the ionization potential of the element that is measured as these determine the number of ions that can be generated from each particle in the plasma as well as the transmission efficiency of ions from the plasma to the detector. However, the baseline also plays an important role. The baseline is composed of the instrument noise (*i.e.* flicker and shot noises), isobaric and polyatomic interferences, and the signal emerging from the dissolved part of the measured isotope [13]. D_{min} of TiO_2 NPs is relatively large because the mass fraction of Ti in TiO_2 is only 59.93% and the total mass of Ti is distributed over several isotopes, with one major (^{48}Ti) and several minor abundances.

In addition, all isotopes of Ti (^{46}Ti, ^{47}Ti, ^{48}Ti, ^{49}Ti and ^{50}Ti) may be interfered by polyatomic compounds (*i.e.* $^{32}S^{16}O$, $^{36}Ar^{12}C$ on ^{48}Ti). In this work we focus on isobaric interferences; specifically, the most abundant isotope, ^{48}Ti (73.72 %), is interfered by an isotope of calcium (^{48}Ca; 0.19 %). While in pure samples this interference would be negligible, in most natural waters Ca appears at orders of magnitude above the concentration of Ti, making this isobaric interference important. Although ^{48}Ti could provide the best D_{min}, the ^{48}Ca signal will dominate the signal at m/z 48 at insufficient mass resolution, increasing the baseline in spICPMS when measuring ^{48}Ti and thus decreasing the accuracy of the measurement. Therefore, in the presence of Ca, the isotopes ^{47}Ti or ^{49}Ti are commonly chosen instead in presence of Ca [15]. Nevertheless, these have much lower abundance (7.44% and 5.41%, respectively) and in combination with the aforementioned factors result in relatively large D_{min} for TiO_2 (*ie* > 90 nm) [14].

The aim of this study is to decrease the D_{min} of TiO_2 NPs, especially in the presence of high calcium concentrations, as is typical for natural waters. Indeed, Gaillardet et *al.* (1999) [16] have shown that, in natural river water, [Ca] varied from *ca.* 2 mg L^{-1} to *ca.* 110 mg L^{-1}. Additionally, Westerhoff et *al.* (2011) [17] have indicated the presence of TiO_2 NPs between 4 and 30 nm in diameter in WWTP effluents that are particularly released into lakes, rivers and streams. Thereby, in this kind of sample, the concentration-translated signal of Ti compared to the concentration of Ca can be insignificant. So, to reduce the D_{min}, we focused on measuring the ^{48}Ti isotope [18]. To differentiate the NPs signal from the background, we proceeded: i) experimentally using either the high or medium resolution mode of an HR-ICP-MS or the tandem MS combined to a reaction cell of an ICP-MS/MS and ii) mathematically using a deconvolution method developed by Cornelis and Hasselöv [13]. The present paper finally critically evaluates the options used to eliminate the interferences, compares these approaches to measuring the ^{47}Ti or ^{49}Ti isotopes instead and proposes the best way to quantify and characterize TiO_2 in the presence of high Ca concentrations.

Experimental Section

Chemicals

Ultrapure water (resistivity ≈ 18.2 MΩ cm^{-1}) from a Millipore Integral 5 (Millipore, Milford, MA, USA) was used throughout the work for dilutions. Mono-elemental standards of Ti and Au at 1 mg mL^{-1} were obtained from SCP Science (Quebec, Canada). Normapure nitric acid (VWR, Radnor, PA, USA) was purified into a sub-boiler DST 1000 (Savillex, Eden Prairie, MN, USA). For the external calibration, all standards were diluted in ultrapure water containing 1% distilled HNO_3.

Synthetic calcium matrix solutions were prepared from a SigmaUltra powder ($Ca(NO_3)_2.4H_2O$; purity > 99.0%, Sigma-Aldrich, Saint-Louis, MO, USA). A 1 L-batch of both solutions at around 5 and 50 mg(Ca) L^{-1} were prepared by dissolution of the precisely weighted powder in Ultrapure water.

Citrate capped AuNPs with a nominal diameter of 60 nm were obtained from British Biocell International (Cardiff, UK). The mean diameter and the concentration provided by the supplier were 59.9 nm with a coefficient of variation of ≤ 8% and $2.60.10^{10}$ particles mL^{-1}, respectively. Before spICPMS measurements, a suspension diluted 10^5 times (NPs number ≈ $2.60.10^5$ particles mL^{-1}) was freshly prepared to calculate the nebulisation efficiency of each ICP-MS using the size method based on the TEM-measured median size of the 60 nm particles. At millisecond dwell times the probability of coincidence decreases by decreasing the concentration. Thus, several AuNPs concentrations have been studied and this concentration was preferred, as it is the highest concentration without particle coincidence.

Sample preparation and verification

A hydrophilic TiO_2 NP powder consisting of rutile coated with an aluminium oxide layer (NM104; Joint Research Centre, IHCP, Ispra, Italy) was used in this study. In order to obtain a stable suspension, 10 mg of the powder was precisely weighted and suspended in 10 mL of ultrapure water in a 15 mL polypropylene centrifugation tube. The suspension was subsequently sonicated for 20 minutes at maximum amplitude with 15 seconds intervals and 1-minute breaks using a sonication probe, Vibracell 100 W (Sonics and Materials Inc., Newton, CT, USA) equipped with a 6 mm microtip. Ice was used to cool down the tube while sonicating. The tube was subsequently centrifuged at 1,750 g for 90 minutes to remove remaining aggregates and large particles (cut-off diameter 40 nm for spheres at 4.23 g cm^{-3} density). Finally, the top 5 mL of the resulting suspension was retained as stock suspension (dispersion methodology development in paragraph SI1 in supporting information). The stock suspension was diluted at several concentrations in both ultrapure water and synthetic calcium matrix solutions previously prepared.

Immediately prior to spICPMS analysis, the Z-average hydrodynamic diameter of the stock suspensions, diluted 10 times in solutions of different Ca concentrations was measured by Dynamic Light Scattering (Nano ZS; Malvern Instruments Ltd., Malvern, UK) to verify that the hydrodynamic diameter remains the same in presence of Ca (data in Table SI2 in supporting information).

Analytical methods

The measurements by spICPMS were performed on 2 different Inductively Coupled Plasma – Mass Spectrometers. The ICP-MS/MS (Agilent 8800, Santa Clara, CA, USA) is a tandem-MS that allows a chemical

resolution of polyatomic and isobaric interferences by using two quadrupoles separated by an octopole reaction cell (ORC). Differences in the reaction kinetics and products between the polyatomic clusters or isobaric isotopes and the gas in the ORC can be used to minimize isobaric interferences. In principle the first quadrupole selects the target m/z where also the specific interference molecules and isotopes will pass together with the target isotope, then in the ORC either the (few) remaining interferences are chemically resolved and the second quadrupole is set to the same m/z as the first or the target isotope is selectively reacted with the cell gas and the second quadruple is set to the adduct m/z thereby removing the remaining interferences. Two reaction gases were tested, oxygen and ammonia. The former gas did not produce ions that were selectively reacting with ^{48}Ti and not with ^{48}Ca (paragraph SI3 in supporting information), whereas ammonia selectively produced reaction product ions with ^{48}Ti. The flow rate of ammonia gas in the ORC was optimized based on the detector response to various Ti concentrations and the intensity of a blank, where the goal was to attain the highest sensitivity, with the lowest background. The reaction product ion ^{63}(TiNH) was chosen for the analysis of TiO_2 NPs. Overall, the ^{48}Ti and ^{48}Ca isotopes are isolated by the first quadrupole and lead in the ORC, where they react with ammonia. The reaction product ^{63}(TiNH) is then isolated with the second quadrupole and collected into the detector, thus eliminating ^{48}Ca. It has to be noted that the ammonia gas used in this system was a mix of ammonia with Helium, in order to minimize risk of damaging the instrumentation due to the corrosive nature of ammonia; an additional 1 mL min^{-1} flow of He gas was also a prerequisite. It is therefore likely that signal suppression occurred due to the presence of He and higher sensitivities can be achieved with a higher purity ammonia gas.

The HR-ICP-MS (Element II, ThermoScientific, Bremen, Germany) enables working in different resolution modes by varying the entrance (*i.e.* before the magnetic field) and the exit (*i.e.* before the detector) ion beam width (Resolution = M/ΔM (*ie*. average mass on mass difference); Low Res. = *ca.* 400, Medium Res. = *ca.* 4,000, and High Res. = *ca.* 10,000). In our case, the theoretical resolution needed to separate ^{48}Ti (m/z = 47.948) from ^{48}Ca (m/z = 47.953) is at least 9,590. Thereby, the separation power of the Element II in high resolution mode is high enough to separate both isotopes.

Daily, both ICP-MS machines were first tuned to ensure maximum sensitivity and stability while also maintaining low uranium oxide formation (UO/U ≤ 5 %) and secondly, high-resolution lenses were optimized in order to reach the best separation of ^{48}Ti and ^{48}Ca on the HR-ICP-MS (screen-shot in Figure SI4 in supporting information) as well as the octopole settings on the ICP-MS/MS. Then, nebulisation and transmission efficiencies were determined. Table 1 gives representative operating conditions and spICPMS parameters for

both instruments. Note that millisecond dwell-times were used in this study, meaning that NPs samples were carefully diluted in order to avoid coincidence.

Standards of dissolved Ti were prepared using the same Ca concentration in which the TiO_2 NPs were measured.

Data treatment

As mentioned in the introduction, the D_{min} increases when the baseline (*i.e.* instrument noise, polyatomic and isobaric interferences and signal emerging from the dissolved element) and particulate signals are of the same order of magnitude. In order to distinguish relatively small NPs from the baseline, first the "conventional data treatment" following the procedure of Pace et *al.* (2011) [12] was applied using the D_{min} as the limit between both signals and secondly the "deconvolution method" was applied to monitored data to reach a better definition of the NPs peak. This method consists of different mathematical correction steps [13] on:

i) *External calibration*. Polya-Gaussian probability mass functions (PG-pmf) are fitted to signal distributions of blanks and dissolved standards. Next, relations between dissolved concentration and pmf parameters (mean, standard deviation and shape) and amongst pmf parameters are established during a regression analysis.

ii) *NPs data*. A PG-pmf is fitted to the relative frequencies of the lowest-intensities of the signal distribution of NP containing samples. The assumption is that these signal intensities stem predominantly from dissolved ions and/or background. Then, the dissolved signal component is subtracted from the total signal and deconvoluted from the resulting signal, effectively arriving at a signal distribution that emerged only from particulate signals and not from dissolved/background ions. Finally, using the established spICPMS theory [12], the particle size distribution is calculated from this signal distribution.

Finally, using the established spICPMS theory [12], the particle mass distribution is calculated from this signal distribution. It was chosen to show distributions of mass per particle instead of size distributions, because the latter requires some assumption of the shape. A spherical shape is usually assumed, but it will be shown that this does not apply to the TiO_2 NPs studied here. Mass distributions were calculated by using the dissolved standards calibration curve to calculate mass per particle from the signal intensities of particle events. The spherical size is proportional to the measured signal intensity with the third root. Direct calculation of spherical size distributions from mass distributions thus results in larger size bins for relatively lower sizes and thus a lower resolution at lower sizes. Some studies choose to rebin size distributions to have equally distributed bins

(e.g. of 1 nm). The numbers of relatively larger sizes increase in this process, because numbers previously assigned to smaller bins are taken together and this occurs more for bins of larger sizes. Size bins were left as is in the present study. Smaller sizes are thus somewhat overrepresented when calculating median sizes compared to larger sizes compared to mass distributions with equally distributed bins.

All these steps were previously programmed in Matlab in the *Nanocount* software. This software is freely available for download at http://blogg.slu.se/nanocount.

Results and discussion

Background, sensitivity and size detection limits (D_{min})

The D_{min} is usually calculated according to the formula from Lee et *al.* [14], assuming a spherical shape of NPs.

$$D_{min} = \left(\frac{6\times(3\sigma)}{R\times f_a\times\rho\times\pi}\right)^{1/3} \quad \textbf{Equation 1}$$

where f_a is the mass fraction of the analysed metallic element in the NP and ρ is the density of the NP, σ (cps) is the standard deviation of the dissolved background signal in the "blank" and R (cps/μg) is the sensitivity of the instrument. Because only one type of NPs is used in our case (TiO_2), the former two parameters can be defined as constants (f_a = 0.5993; ρ = 4.23 g cm^{-3}). Thereby, D_{min} is essentially determined by R and by the 3σ criterion, assuming that the signal of a particle is detectable above 3 times the standard deviation of the background. Note that D_{min} is inversely proportional to R, because an increase in sensitivity also results in an increase in the average dissolved background intensity. In the current study, the 3σ in ultra-pure water and at different calcium concentration as well as the sensitivity (R) measuring the intensity ^{47}Ti, ^{48}Ti and ^{49}Ti using titanium dissolved standards having different background concentrations of Ca were experimentally determined (Table 2). First, a conventional calibration curve (mass vs average intensity) was used in order to determine the slope of ionic Ti standards solution (K). Then, R was calculated for each condition using the relation R = K / η, where η is the nebulisation efficiency [14] (see an example calculation in supporting information SI9). It will be argued later that equation (1) is not appropriate when using a deconvolution method to distinguish dissolved and particulate signals, but equation (1) is still deemed appropriate for the purpose of comparing different instrumental approaches to measure Ti.

Table 2 shows that, as expected, ^{48}Ti sensitivity is much higher than for other isotopes due to its higher abundance. Also, the sensitivity of the HR-ICP-MS is higher compared to the response of the ICP-MS/MS. Nevertheless, regardless the isotope measured, both ICP-MS sensitivities are not affected by the rise of calcium

concentration. Conversely, the increase of calcium concentration produces an increasing background for ^{48}Ti. In medium resolution (MR), even if polyatomic interferences (*i.e.* $^{32}S^{16}O$, $^{36}Ar^{12}$) are correctly resolved because of the quite large mass difference, ^{48}Ca is not sufficiently separated from ^{48}Ti. Indeed, a resolution of 4,000 is sufficient for polyatomic interferences when a resolution higher than 9,590 is needed to fully resolve the ^{48}Ca isobaric interference. The Ti signal intensities therefore overlap significantly with background signals that are mainly caused by Ca ions. In high resolution (HR > 10,000 (screen-shot in Figure SI4 in supporting information)) the resolution is higher than MR resulting in lower background counts, but the broad ^{48}Ca peak still interferes significantly with the ^{48}Ti signals and more so as the Ca concentration increases. Thus, the raise of calcium concentration produces an increase of the background signal and hence its noise leading to a rise of the 3σ. Note also that the standard deviation of background signals is also increased in some cases by drift of the signal and accidentally measured nanoparticle events in blank samples because of carry-over of previous measurements.

On the ICP-MS/MS, the gas addition in the ORC effectively removes the Ca interference, even at calcium concentrations up to 50 mg L^{-1}. For other isotopes, the average background intensity does increase with the Ca concentration. Nevertheless, in all ICP-MS/MS conditions and for ^{47}Ti and ^{49}Ti in HR-ICP-MS, even if the background signal is not affected, the higher the concentration of calcium, the poorer is the stability and so, higher is the 3σ. Gillson et *al.* [19] assign this so called "matrix effect" to changes in the flux and the composition of the ion beam that cause space charges after the skimmer cone and thus perturbations for all measured isotopes.

All size detection limits (D_{min}) calculated using the Equation 1 are presented in Figure 1 as a function of the Ca concentration. Because sensitivities remain constant at different calcium concentrations, D_{min} are all evaluated using R at [Ca] = 0 mg L^{-1}. This means that calculated D_{min} values are only dependant on the value of 3σ in our case. As explained above, it appears that the complication of the matrix affects the background signal and thus the background noise causing an increase of the standard deviation of the background. Thereby, regardless the isotope, the D_{min} increases as the calcium concentration rises. However the sensitivity of the HR-ICP-MS or the low background of the ICP-MS/MS almost always lead to better D_{min} compared to that from Lee et *al.* for TiO_2 NPs [14]. D_{min} is higher to that found in the latter publication in the case of ^{47}Ti without gas addition on the ICP-MS/MS, which is thus far the most used method to analyse Ti in a Ca containing matrix [15]. Similarly, measuring ^{48}Ti in MR on the HR-ICP-MS and ^{48}Ti adding NH_3 on the ICP-MS/MS, both at [Ca] = 50 mg L^{-1}, leads to higher D_{min}. Thus, using these latter conditions at a higher calcium concentration (*i.e.* [Ca] = 100 mg L^{-1})

would have lead to D_{min} higher than 90 nm. Also, irrespectively of the ICP-MS instrument used, lower size detection limits are achieved when measuring ^{48}Ti, due to the lower abundance of ^{47}Ti or ^{49}Ti, compared to ^{48}Ti. Moreover, although the HR-ICP-MS background increases rapidly in presence of calcium, it appears that measuring ^{48}Ti in high resolution allows measuring smaller TiO_2 NPs than in any other conditions at concentration up to [Ca] = 100 mg L^{-1}.

Thereby, only ^{48}Ti data using either the high-resolution mode or the ammonia addition were used for further analysis, due to the improved detection limits attained measuring this isotope.

Detection of TiO_2 NM104 in calcium matrix by spICPMS

Experimental resolution of the background.

Figure 2 shows the mass distribution of blanks and NM104 suspensions measured with the HR-ICP-MS instrument. Also shown is $Mass_{min}$, (*i.e.* the mass corresponding to the D_{min} (3σ of the blank)). As explained in the paragraph above, even if ^{48}Ti is separated from ^{48}Ca using the high resolution mode, the mode intensity (*i.e.* the intensity that appears most often in the set of data) of the blank clearly increases with Ca concentration. It also appears that increasing the Ca concentration also increases the mode signal intensity of the NM104 containing samples. Distinction of dissolved and particulate signals is straightforward if all particulate signals are larger than all dissolved signals so that separate peaks emerge in the signal distribution histograms. However, Figure 2 shows that none of the particle containing samples exhibits multiple peaks. Dissolved and particulate signals therefore overlap in all cases, even at 0 mg L^{-1} Ca. In addition, the difference in signal intensities between blank and NM104 signals reduces as the Ca concentration increases. Indeed, while the concentration of calcium rises, NPs become more and more included with the dissolved fraction. A data analysis method commonly used to separate dissolved background from particle events consists of using the standard deviation of the baseline [20]. The NPs signal is calculated based on the number of outliers and is then applied on the sample histogram, where all events higher than the "n x sigma" are considered as particles. The main issue with this method is that the algorithm biases the "cut-off" value by randomly taking particle events as false negative (*i.e.* part of the baseline) or taking baseline instability as false positive (*i.e.* particle event) (values in Table SI5 in supporting information). In this study, the $Mass_{Min}$ "cut-off" *i.e* the mass detection limit in each condition is applied. In Figure 2, compared to the reference mass distribution at Ca = 0 mg L^{-1}, it seems that the mass distribution at Ca = 5 mg L^{-1} is almost not affected. Indeed, the mass distributions for both calcium concentrations follow an identical log-normal evolution and show a constant mode mass (*i.e.* the mass that appears most often in the set of data) (Table 3). Conversely, at Ca = 50 mg L^{-1} and 100 mg L^{-1}, even if the log-

normal evolution is still observable (Figure 2), the higher cut-off hides the majority of the particle population and results in higher mode masses (Table 3). Moreover, the total particle number concentrations are constant for Ca = 0 mg L^{-1} and Ca = 5 mg L^{-1} but decrease at higher concentrations (Table 3), showing that, in our study, the "conventional data treatment" only works up to Ca ≤ 5 mg L^{-1} on the HR-ICP-MS. In order to better discriminate the signal of ^{48}Ti from the ^{48}Ca background, a deconvolution data treatment method was applied.

Figure 3 shows the mass distribution for blanks and the TiO_2 NM104 suspensions dispersed in different calcium solutions obtained using ICP-MS/MS. The lower sensitivity of the ICP-MS/MS results in a poorer resolution in terms of the mass distribution (larger mass bins, compared to the HR-ICP-MS data). Compared to the HR-ICP-MS, a similar log-normal evolution is still noticeable but the high cut-off prevents the observation of the smallest TiO_2 NPs. The mode mass is also higher in this case, resulting in higher equivalent size (Tables 3 and 4) and the total particle number concentration decreases as calcium concentration increases. Here, we also applied the deconvolution data treatment method to improve the quality of the distribution.

Mathematical correction of the background (deconvolution method).

Figure 4 shows the TiO_2 mass distribution for NM 104 suspensions in calcium matrixes for the HR-ICP-MS measurements and Figure 5 shows the TiO_2 mass distribution for the ICP-MS/MS measurements after deconvolving data (deconvolution fits in Figure SI6a and SI6b in supporting information). It clearly appears that using the deconvolution method, particle events previously lower than $Mass_{min}$ are retained in the mass distributions obtained on both instruments. Indeed, for all Ca ≥ 5 mg L^{-1} the particle mass distribution remains the same as with Ca = 0 mg L^{-1}. Moreover, the total particle number concentration is more constant when regarding the results of both ICP-MS instruments separately (Table 3 and 4). This confirms that the deconvolution data treatment allows a better discrimination between Ca background and Ti signal and thus, reduces the confounding effect of the rise of Ca concentrations.

However, both ICP-MS instruments do not give the same mass distribution. Indeed, the ICP-MS/MS results give a considerably higher equivalent spherical median size and an order of magnitude lower total particle number concentrations (Table 3 and 4). These differences are due to the lower sensitivity and thus higher size detection limits of the ICP-MS/MS (Figure 1) regardless of Ca concentration (Table 2). Thus, the smallest sized TiO_2 population cannot be detected by the ICP-MS/MS causing an under-estimation of the number concentrations and an over-estimation of the mode particle size. However, using the deconvolution, Table 4 shows a lower total particle number concentration than the one using the D_{min}, an observation that shows that the deconvolution method also removes particulate signals by misrepresenting the dissolved data at low sensitivity.

Equation 1 is appropriate when discerning dissolved and particulate signals using a single cut-off value such as the one produced by the D_{min} or by the more commonly used "n x sigma method" [20]. However, Figures 4 and 5 show at least a part of the intensities lower than $Mass_{min}$ are identified as particles using the deconvolution approach, leading to a lower D_{min} compared to Figures 2 and 3 [13]. The D_{min} is not determined by the standard deviation of the blank when using a deconvolution, because this standard deviation is modelled based on the calibration standards when fitting the PG-pmf model to a particle containing sample. The D_{min} is rather determined by the accuracy of this fitting process. The accuracy decreases with drift or other noise sources that cannot be predicted by the PG-pmf model [21] and increases with the number of fit points that can be used to establish the signal distribution of the dissolved background in a particulate sample. The number of fit points had to be limited to two in this case, the theoretical minimum [13], because it is clear that even some of the lowest intensity signals are caused by particles, especially in the case of the ICP-MS/MS data. Rigorous calculation of the D_{min} in this case would have to rely on a bootstrap procedure to quantify how the intrinsic data variability may result in different PG-pmf models. Bootstrapping involves randomly selecting smaller subsets of data from a larger dataset with replacement. This procedure thus creates resampled replicate particle size distributions from the larger dataset allowing quantifying the standard deviation introduced by the subsequent deconvolution algorithm steps. The D_{min} would then correspond to the signal intensity where average bootstrapped dissolved frequency fitted to the total histogram is significantly different from the average bootstrapped particle histogram frequency. This calculation is beyond the scope of the current publication, but the consistency of the total particle number concentration support the claim that applying the deconvolution method improves the calculation of D_{min} and the lowest detectable particle size was achieved by combining ^{48}Ti measurements using the HR-ICP-MS in HR mode and the deconvolution algorithm.

Method validation

In order to assess the quality of the results obtained after deconvolution, ^{48}Ti (HR) data acquired on the HR-ICP-MS were compared to NM104 characterisation using several different methods by several European laboratories participating to the NANOGENOTOX Joint Action, as well as by the JRC [22]. Indeed, the spICPMS technique does not provide all information about the particle and another analytical tool is useful especially to determine its morphology. Undeniably, the determination of the particle size distribution is correct only if the shape of the particles is known, otherwise the size calculated is biased ($eds_{Deconvolution}$ in Table 3 and 4) and only an equivalent diameter for sphere can be established (Figure SI7a and SI7b in the supporting information). Nevertheless, in this report, the particle morphology is described varying from equidimensional euhedral to

elongated. Thereby, a first assumption can be made by assuming a prolate ellipsoid shape and thus, using the following formula for the calculation of the volume:

$$V = {}^{4}/_{3} \times \pi \times x^2 \times z \qquad \text{Equation 2}$$

where V is the volume of the particle in nm^3 and *x* is the short dimension and *z* is the long dimension in nm. The primary particles of TiO_2 NM-104 have been shown based on TEM data to be *ca.* 25 nm along the smaller dimension (*i.e* the 1st dimension: *x*) [22]. Then, a second assumption is made by assuming a prolate ellipsoidal shape, fixing the *x* dimension at 25 nm and using the mass distribution shown in Figure 6, a size distribution of the 3rd dimension (*z*) can be estimated from equation (3):

$$z_i = \frac{3 \times m_i}{4 \times \rho \times x^2} \qquad \text{Equation 3}$$

where m_i is the mass of the TiO_2 mass distribution in g in the i^{th} bin, ρ is the density of the nanoparticle (ρ_{TiO2} = $4{,}23 \times 10^{-21}$ g nm^{-3}) and *x* is equal to 25 nm.

Previous characterisation using TEM [22] of the median aspect ratio of NM104 is *ca.* 1.6. Using 25 nm for the smallest dimension, the median largest dimension should be 40 nm. Figure 6 displays the calculated size distribution for the 3rd dimension (*z*) at the different calcium concentrations. It clearly appears in Table 3 that the largest dimension size distributions calculated with HR-ICP-MS data are realistic for all calcium solutions especially because the mode size at the maximum particle concentration in all conditions does not vary, whereas the median *z* dimension calculated using ICP-MS/MS measurements is unrealistic (Table 4).

Conclusion

The application of HR-spICP-MS and spICP-MS/MS for the calculation of D_{min} used here allowed for a decrease of the limit between dissolved and particulate signals. This method can be readily applied to natural samples by removing particles from the sample (using an ultra-filtration or ultra-centrifugation) and thus measuring only the dissolved signal as the "blank". D_{min} would then be calculated based on the dissolved signal in the sample itself. However, this method induces false negatives as it does not count small NPs when the background is high and in our case a data analysis method (*i.e.* deconvolution) had to be applied. Lower detection limits were achieved in this work for TiO_2 NPs in a highly concentrated background of calcium using single-particle ICP-MS by combining i) the measurement of the ^{48}Ti isotope instead of ^{47}Ti or ^{49}Ti, ii) the use of the high resolution mode of a HR-ICP-MS to separate ^{48}Ti from ^{48}Ca, and iii) the application of a deconvolution method to separate the truly nanoparticulate signal from the residual background of ^{48}Ca when calcium concentrations are high (>50 mg L^{-1}). Alternatively, for particles above 64 nm, a spICP-MS/MS instrument can

be used in the reaction mode with ammonia as a reaction gas. This approach resolves the majority of ^{48}Ca interference on ^{48}Ti, however sensitivity is reduced by the need to introduce He along with ammonia, to protect equipment against the corrosive nature of the ammonia.

Another way to resolve NPs signal from the baseline needs to be investigated by using microsecond dwell-time even if, there is no guarantee that the detection limits will be improved. Indeed, as Montano et *al.* (2014) [25] have shown, the NPs data at the boundary of the baseline could be lost due to a decrease of the intensity of the decomposed event. Nevertheless, the combination of a high sensitivity ICP-MS with microsecond dwell-times could be promising.

Another step forward in the detection of TiO_2 NPs would be to distinguish engineered and natural ones using another element present in engineered NPs. For instance, manufactured TiO_2 NPs usually have a layer of alumina in order to improve their stability. So, by simultaneously measuring Al and Ti using either an ICP-TOF-MS [23] or a Mattauch-Herzog geometry ICP-MS [24], the distinction between natural and engineered TiO_2 NPs would be facilitated. However, ion extraction and detection of this kind of ICP-MS must be improved in order to reach lower detection limits.

References

1. Shi, H., Magaye, R., Castranova, V., & Zhao, J., Titanium dioxide nanoparticles: a review of current toxicological data, *Particle and Fibre Toxicology* 10 (2013) 1-33.
2. Keller, A. A., McFerran, S., Lazareva, A., & Suh, S., Global life cycle releases of engineered nanomaterials, *Journal of Nanoparticle Research* 15 (2013) 1692.
3. Lin, X., Li, J., Ma, S., Liu, G., Yang, K., Tong, M., & Lin, D., Toxicity of TiO_2 Nanoparticles to *Escherichia coli*: Effects of Particle Size, Crystal Phase and Water Chemistry, *PLoS ONE* 9 (2014) 1-8.
4. Shang L, Nienhaus K, N. G., Engineered nanoparticles interacting with cells: size matters., *J Nanobiotechnology.* 12 (2014) .
5. Domingos, R. F., Baalousha, M. A., Ju-Nam, Y., Reid, M. M., Tufenkji, N., Lead, J. R., Leppard, G. G., & Wilkinson, K. J., Characterizing Manufactured Nanoparticles in the Environment: Multimethod Determination of Particle Sizes, *Environmental Science & Technology* 43 (2009) 7277-7284.
6. Lopez-Serrano, A., Olivas, R. M., Landaluze, J. S., & Camara, C., Nanoparticles: a global vision. Characterization, separation, and quantification methods. Potential environmental and health impact, *Anal. Methods* 6 (2014) 38-56.
7. da Silva, B. F., Perez, S., Gardinalli, P., Singhal, R. K., Mozeto, A. A., & Barcelo, D., Analytical chemistry of metallic nanoparticles in natural environments, *TrAC Trends in Analytical Chemistry* 30 (2011) 528 - 540.
8. Donovan, A. R., Adams, C. D., Ma, Y., Stephan, C., Eichholz, T., & Shi, H., Single particle ICP-MS characterization of titanium dioxide, silver, and gold nanoparticles during drinking water treatment, *Chemosphere* 144 (2016) 148 - 153.
9. Tuoriniemi, J., Cornelis, G., & Hassellov, M., A new peak recognition algorithm for detection of ultra-small nano-particles by single particle ICP-MS using rapid time resolved data acquisition on a sector-field mass spectrometer, *J. Anal. At. Spectrom.* 30 (2015) 1723-1729.
10. Mitrano, D. M., Ranville, J. F., Bednar, A., Kazor, K., Hering, A. S., & Higgins, C. P., Tracking dissolution of silver nanoparticles at environmentally relevant concentrations in laboratory, natural, and processed waters using single particle ICP-MS (spICP-MS), *Environ. Sci.: Nano* 1 (2014) 248-259.
11. Degueldre, C., Favarger, P.-Y., & Wold, S., Gold colloid analysis by inductively coupled plasma-mass spectrometry in a single particle mode, *Analytica Chimica Acta* 555 (2006) 263 - 268.
12. Pace, H. E., Rogers, N. J., Jarolimek, C., Coleman, V. A., Higgins, C. P., & Ranville, J. F., Determining transport efficiency for the purpose of counting and sizing nanoparticles via single particle inductively coupled plasma mass spectrometry, *Analytical Chemistry* 83 (2011), 9361–9369.
13. Cornelis, G. & Hassellov, M., A signal deconvolution method to discriminate smaller nanoparticles in single particle ICP-MS, *J. Anal. At. Spectrom.* 29 (2014) 134-144.
14. Lee, S., Bi, X., Reed, R. B., Ranville, J. F., Herckes, P., & Westerhoff, P., Nanoparticle Size Detection Limits by Single Particle ICP-MS for 40 Elements, *Environmental Science & Technology* 48 (2014) 10291-10300.
15. Gondikas, A. P., von der Kammer, F., Reed, R. B., Wagner, S., Ranville, J. F., & Hofmann, T., Release of TiO2 Nanoparticles from Sunscreens into Surface Waters: A One-Year Survey at the Old Danube Recreational Lake, *Environmental Science & Technology* 48 (2014) 5415-5422.
16. Gaillardet, J., Dupré, B., Louvat, P., & Allègre, C. J., Global silicate weathering and CO_2 consumption rates deduced from the chemistry of large rivers, *Chemical Geology* 159 (1999) 3 - 30.
17. Westerhoff, P., Song, G., Hristovski, K., & Kiser, M. A., Occurrence and removal of titanium at full scale wastewater treatment plants: implications for TiO_2 nanomaterials, *J. Environ. Monit.* 13 (2011) 1195-1203.
18. Dan, Y., Shi, H., Stephan, C., & Liang, X., Rapid analysis of titanium dioxide nanoparticles in sunscreens using single particle inductively coupled plasma--mass spectrometry, *Microchemical Journal* 122 (2015) 119 - 126.
19. Gillson, G. R., Douglas, D. J., Fulford, J. E., Halligan, K. W., & Tanner, S. D., Nonspectroscopic interelement interferences in inductively coupled plasma mass spectrometry, *Analytical Chemistry* 60 (1988) 1472-1474.
20. Tuoriniemi, J., Cornelis, G., & Hassellöv, M., Size Discrimination and Detection Capabilities of Single-Particle ICPMS for Environmental Analysis of Silver Nanoparticles, *Analytical Chemistry* 84 (2012) 3965-3972.
21. Cornelis, G. & Rauch, S., Drift correction of the dissolved signal in single particle ICPMS, *Analytical and Bioanalytical Chemistry* 408 (2016) 5075--5087.
22. Kirsten Rasmussen, Jan Mast, P.-J. D. T. E. V. N. W. F. V. S. J. C. P. L. D. T. E. V. D. K. A. J. R. B. M. L. S. H. N. I. K. K. P. A. C. V. K.-S. Y. K. N. T. O. S. C. G. D. R. O. W. S. B. B. B. C. M. B. S. L. D. R. N. D. N. M. T. O. P. S. B. D. G. F. P. G. C. V. S. G. C. N. G. C. G. & Mech, A., Titanium Dioxide, NM-100, NM-101, NM-102, NM-103, NM-104, NM-105: Characterisation and Physico- Chemical Properties, *JRC Science and Policy Reports* (2014) .

23. Praetorius, A., Gundlach-Graham, A., Goldberg, E., Fabienke, W., Navratilova, J., Gondikas, A., Kaegi, R., Günther, D., Hofmann, T., and von der Kammer, F., Single-particle multi-element fingerprinting (spMEF) using inductively-coupled plasma time-of-flight mass spectrometry (ICP-TOFMS) to identify engineered nanoparticles against the elevated natural background in soils, *Environ. Sci.: Nano,* (2017) 307-314.
24. Barnes, Schilling, G. D., Sperline, R., Denton, M. B., Young, E. T., Barinaga, C. J., Koppenaal, D. W., & Hieftje, G. M., Characterization of a Focal Plane Camera Fitted to a Mattauch−Herzog Geometry Mass Spectrograph. 2. Use with an Inductively Coupled Plasma, *Analytical Chemistry* 76 (2004) 2531-2536.
25. Montaño, M. D., Badiei, H. R., Bazargan S., and Ranville, J. F., Improvements in the detection and characterization of engineered nanoparticles using spICP-MS with microsecond dwell times, *Environ. Sci.: Nano,* (2014) 338-346.

Figures and Tables

Table 1. ICP-MS operating conditions and spICPMS parameters.

Table 2. Calculated backgound (cps +/- 3σ) and sensitivity (cps/μg) of each isotope for both ICP-MS at different Calcium concentrations.

Table 3. Data (n = 1) obtained with the HR-ICP-MS at the different calcium concentrations.

Table 4. Data (n = 1) obtained with the ICP-MS/MS at the different calcium concentrations.

Figure 1. Theoretical size detection limit (D_{min}) for each isotope on both ICP-MS at different Calcium concentrations.

Figure 2. Graphs of Particle Number Concentration (mL^{-1}) vs. Mass (g) for the HR-ICP-MS results.

Figure 3. Graphs of Particle Number Concentration (mL^{-1}) vs. Mass (g) for the ICP-MS/MS.

Figure 4. Graphs of Particle Number Concentration (mL^{-1}) vs. Mass (g) for the HR-ICP-MS determined with the Deconvolution method.

Figure 5. Graphs of Particle Number Concentration (mL^{-1}) vs. Mass (g) for the ICP-MS/MS determined with the Deconvolution method.

Figure 6. Graphs of Particle Number Concentration (mL^{-1}) vs. 3rd dimension of the ellipsoid (nm) based on data measured with HR-ICP-MS.

Table 1. ICP-MS operating conditions and spICPMS parameters.

Parameter (unit)	HR-ICP-MS	ICP-MS/MS
Spray chamber type	Quartz cyclonic	Quartz cyclonic
Nebulizer type	PFA MicroFlow	PFA MicroFlow
Plasma power (W)	1315	1550
Cool Gas (L min^{-1})	16	15
Auxiliary Gas (L min^{-1})	1	1
He gas (mL min^{-1})	NA	1
NH_3 gas (%)	NA	10
Sample Gas (L min^{-1})	0.95	0.80
Sample uptake (µL min^{-1})	220	210
Monitored isotope	^{47}Ti, ^{48}Ti and ^{49}Ti	^{47}Ti and $^{63}(TiNH)$
Dwell time (ms)	5	3
Number of dwell time	10000	35713
Transmission efficiency (%)	MR = 7 ; HR = 1	7

Table 2. Calculated background (cps +/- 3σ) and sensitivity (cps/µg) of each isotope for both ICP-MS at different Calcium concentrations. NA means that the data was not acquired. Signal to Background ratios are available in supporting information (SI8).

	HR-ICP-MS								ICP-MS/MS			
[Ca]	^{47}Ti (MR)		^{48}Ti (MR)		^{49}Ti (MR)		^{48}Ti (HR)		^{47}Ti (No Gas)		^{48}Ti (NH_3)	
mg/L	Background	Sensitivity	Background	Sensitivity	Background	Sensitivity	Background	Sensitivity	Background	Sensitivity	Background	Sensitivity
	cps +/- 3σ	cps/µg	cps +/- 3σ	cps/µg	cps +/- 3σ	cps/µg	cps +/- 3σ	cps/µg	cps +/- 3σ	cps/µg	cps +/- 3σ	cps/µg
0	13 +/- 228	$1.2x10^{13}$	1399 +/- 5981	$1.8x10^{14}$	81 +/- 1511	$1.0x10^{13}$	25 +/- 815	$1.4x10^{14}$	35 +/- 424	$2.2x10^{11}$	13 +/- 264	$1.1x10^{12}$
5	75 +/- 667	$1.7x10^{13}$	129542 +/- 101895	$2.1x10^{14}$	57 +/- 3196	$1.3x10^{13}$	2414 +/- 8037	$1.5x10^{14}$	35 +/- 419	$2.4x10^{11}$	16 +/- 375	$1.2x10^{12}$
50	NA	NA	892794 +/- 552998	$2.1x10^{14}$	NA	NA	29361 +/- 36471	$1.0x10^{14}$	NA	NA	52 +/- 973	$1.4x10^{12}$
100	NA	NA	NA	NA	NA	NA	52914 +/- 57691	$1.6x10^{14}$	NA	NA	NA	NA

Table 3. Data (n = 1) obtained with the HR-ICP-MS at the different calcium concentrations. The mode mass (x 10^{-16} g), its equivalent diameter for sphere "eds" (nm) and the total particle number concentration [TiO_2] (x 10^6 mL^{-1}) calculated using the $Mass_{Min}$ cut-off and the Deconvolution, respectively. The instrumental error associated to the mode mass and to sizes is *ca.* 10%.

[Ca] (mg/L)	$m_{MassMin}$ (x 10^{-16} g)	$eds_{MassMin}$ (nm)	$[TiO_2]_{MassMin}$ (x 10^6 mL^{-1})	$m_{Deconvolution}$ (x 10^{-16} g)	$eds_{Deconvolution}$ (nm)	$[TiO_2]_{Deconvolution}$ (x 10^6 mL^{-1})	$z_{Ellipsoid}$ (nm)
0	0.27	23	3.38	0.44	27	3.83	35
5	0.27	23	4.10	0.54	29	5.21	38
50	1.60	41	1.18	0.53	29	3.00	38
100	2.29	47	2.35	0.48	28	3.94	39

Table 4. Data (n = 1) obtained with the ICP-MS/MS at the different calcium concentrations. The mode mass (x 10^{-16} g), its equivalent diameter for sphere "eds" (nm) and the total particle number concentration [TiO_2] (x 10^6 mL^{-1}) calculated using the $Mass_{Min}$ cut-off and the Deconvolution, respectively. The instrumental error associated to the mode mass and to sizes is *ca.* 10%.

[Ca] (mg/L)	$m_{MassMin}$ (x 10^{-16} g)	$eds_{MassMin}$ (nm)	$[TiO_2]_{MassMin}$ (x 10^6 mL^{-1})	$m_{Deconvolution}$ (x 10^{-16} g)	$eds_{Deconvolution}$ (nm)	$[TiO_2]_{Deconvolution}$ (x 10^6 mL^{-1})	$z_{Ellipsoid}$ (nm)
0	16.14	90	1.04	7.60	70	0.41	570
5	16.69	91	0.92	6.66	67	0.38	550
50	23.50	102	0.49	6.96	68	0.40	480

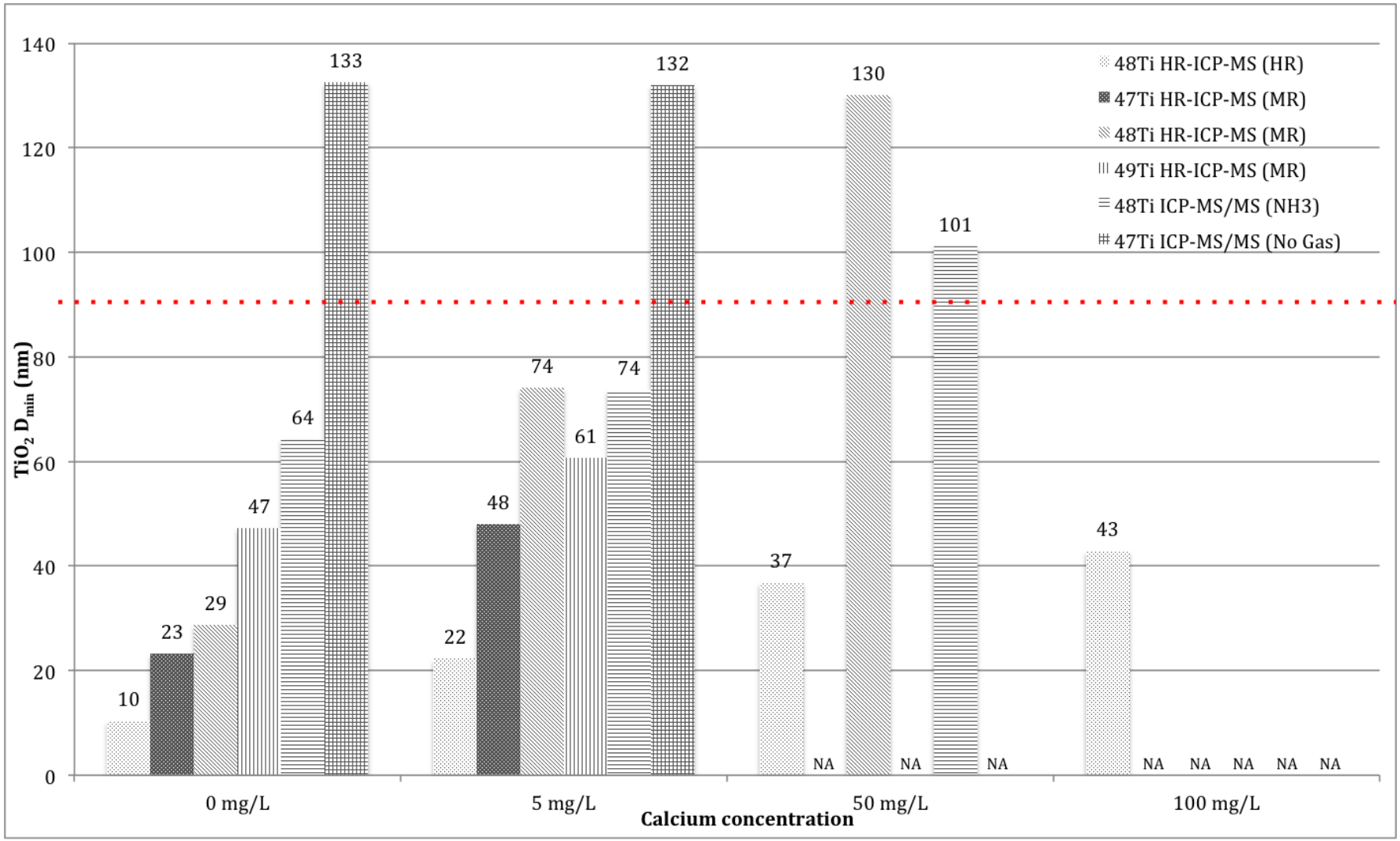

Figure 1. Theoretical size detection limit (D_{min}) for each isotope on both ICP-MS at different Calcium concentrations. Black dots bar: ^{48}Ti (HR) on HR-ICP-MS; White dots bar: ^{47}Ti (MR) on HR-ICP-MS; Oblique lines bar: ^{48}Ti (MR) on HR-ICP-MS ; Vertical lines bar: ^{49}Ti (MR) on HR-ICP-MS ; Horizontal lines bar: ^{48}Ti (NH_3) on ICP-MS/MS ; Gridded bar: ^{47}Ti (No Gas) on ICP-MS/MS . The red dotted line represents the size detection limit calculated by Lee et *al.* on ^{47}Ti in ultrapure water. NA means that the data was not acquired.

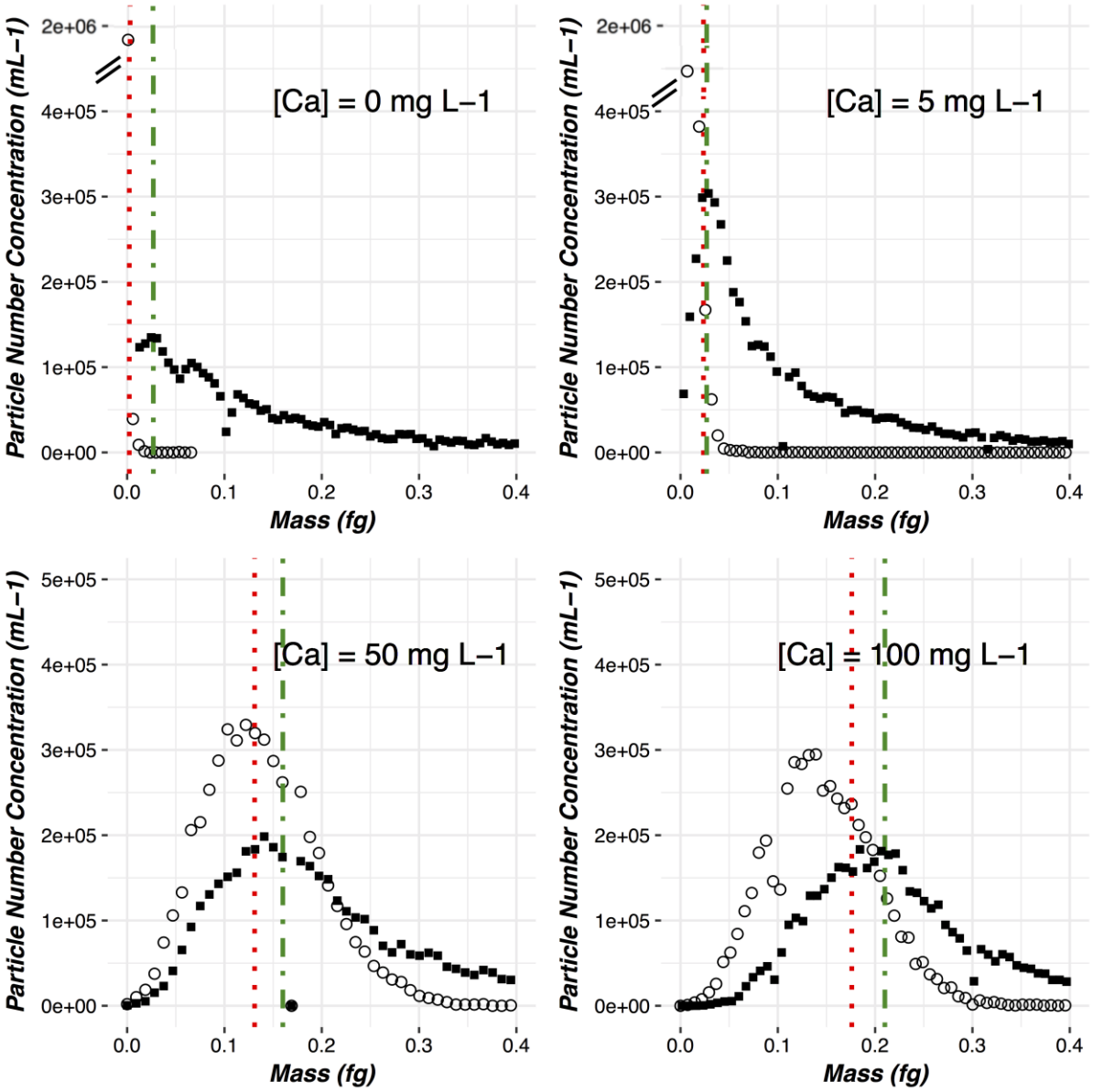

Figure 2. Graphs of particle number concentration (mL^{-1}) vs. mass (g) measured with the HR-ICP-MS instrument. Circles represent the particle mass distribution of blanks and squares represent the particle mass distribution of TiO_2 NM104 solutions in Ultrapure water (top left), 5 mg(Ca) L^{-1} (top right), 50 mg(Ca) L^{-1} (bottom left) and 100 mg(Ca) L^{-1} (bottom right). The red dotted line represents $Mass_{min}$ calculated based on equation (1) and the green dotted line represents the mode mass ($m_{MassMin}$ in Table 3).

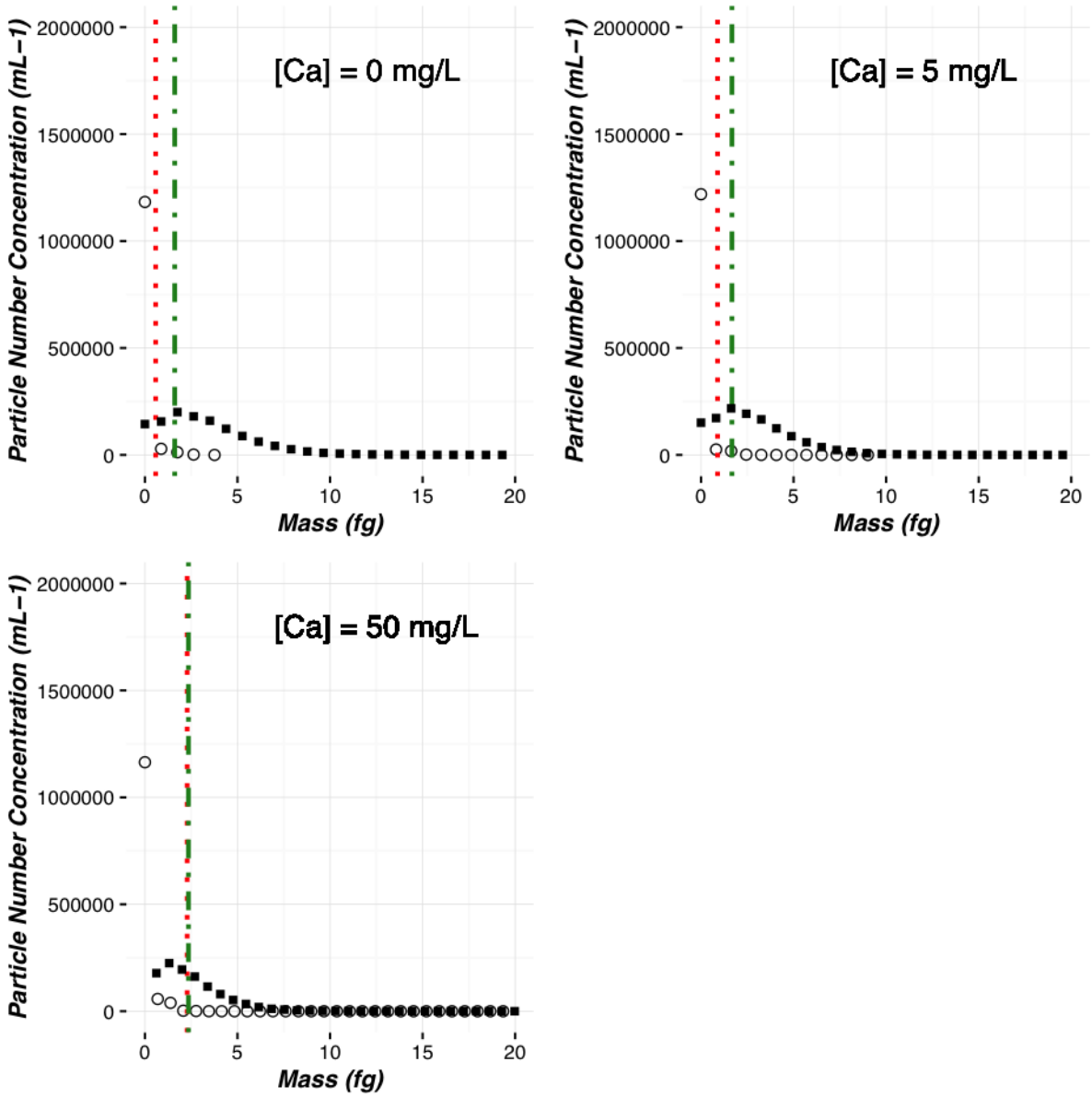

Figure 3. Graphs of particle number concentration (mL^{-1}) vs. mass (g) using the ICP-MS/MS instrument. Circles represent the particle mass distribution of blanks and squares represent the particle mass distribution of TiO_2 NM104 solutions in Ultrapure water (top left), 5 mg(Ca) L^{-1} (top right), and 50 mg(Ca) L^{-1} (bottom). The red dotted line represents the $Mass_{min}$ calculated based on equation (1) and the green dotted line represents the mode mass ($m_{MassMin}$ in Table 3).

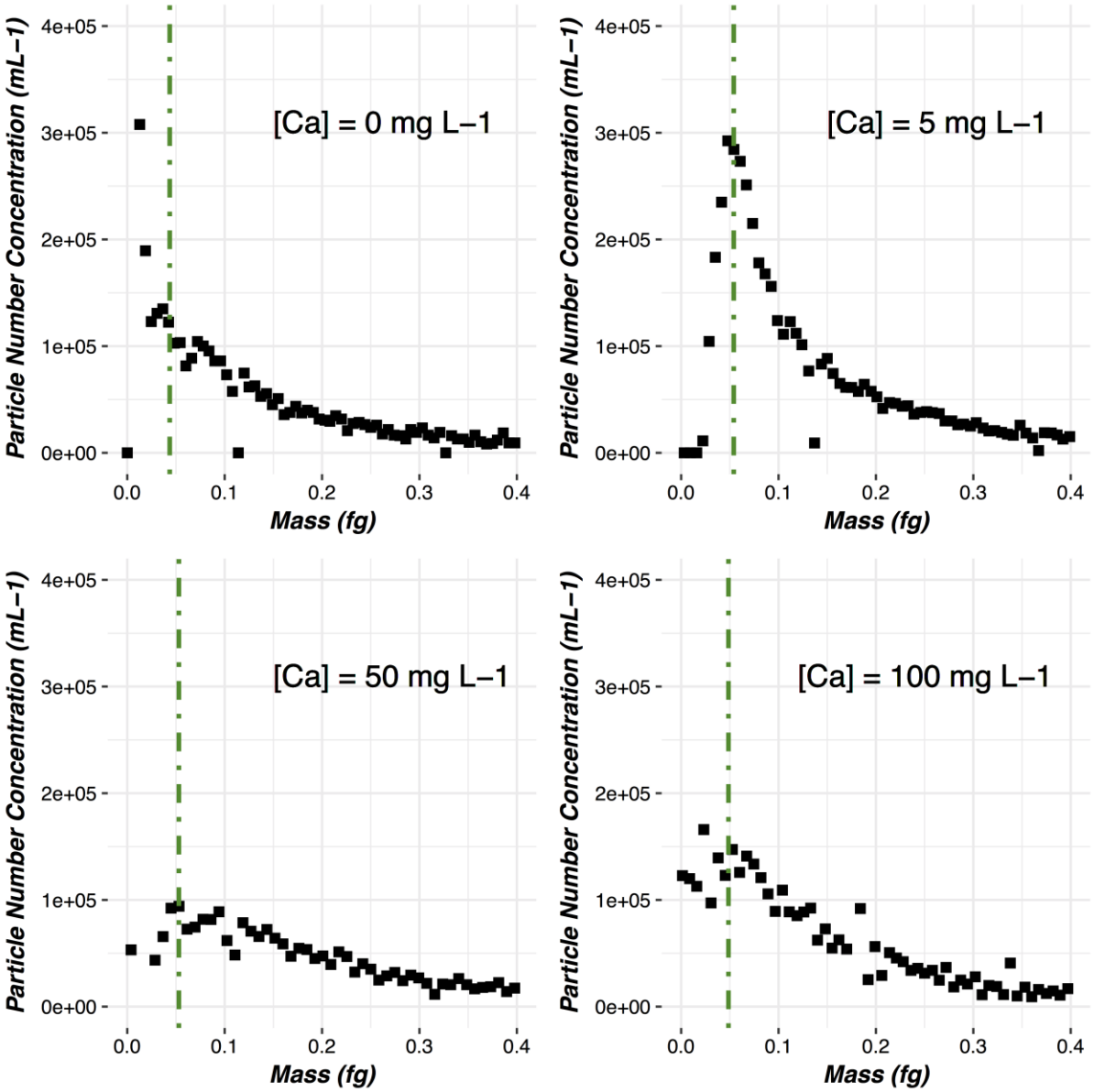

Figure 4. Graphs of particle number concentration (mL^{-1}) vs. mass (g) using the HR-ICP-MS instrument determined with the deconvolution method. Squares represent the particle mass distribution of TiO_2 NM104 solutions in Ultrapure water (top left), 5 mg(Ca) L^{-1} (top right), 50 mg(Ca) L^{-1} (bottom left) and 100 mg(Ca) L^{-1} (bottom right). The green dotted line represents the mode mass ($m_{Deconvolution}$ in Table 3).

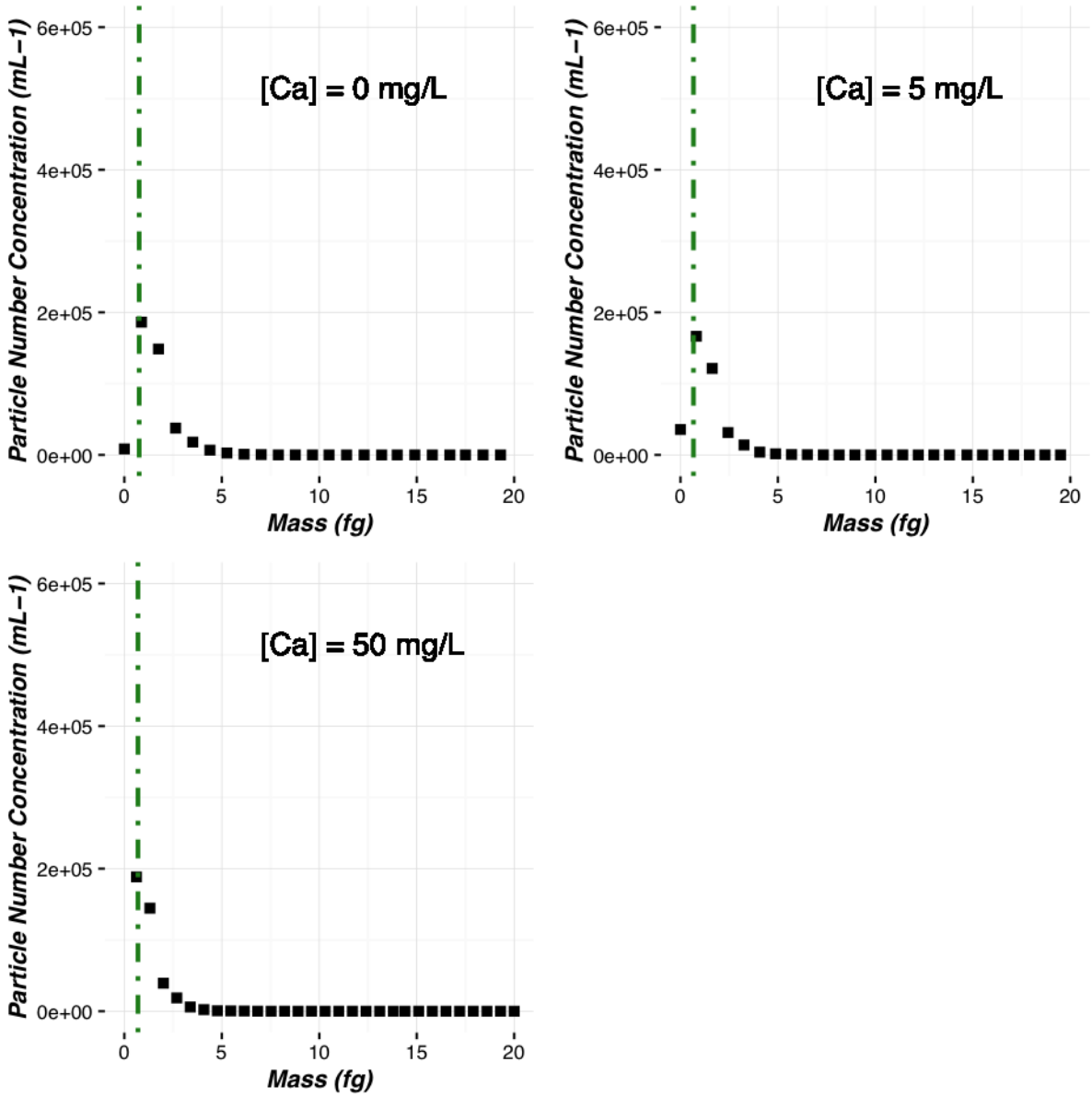

Figure 5. Graphs of particle number concentration (mL^{-1}) vs. mass (g) using the ICP-MS/MS instrument, determined with the deconvolution method. Squares represent the particle mass distribution of TiO_2 NM104 solutions in Ultrapure water (top left), 5 mg(Ca) L^{-1} (top right), and 50 mg(Ca) L^{-1} (bottom). The green dotted line represents the mode mass ($m_{Deconvolution}$ in Table 3).

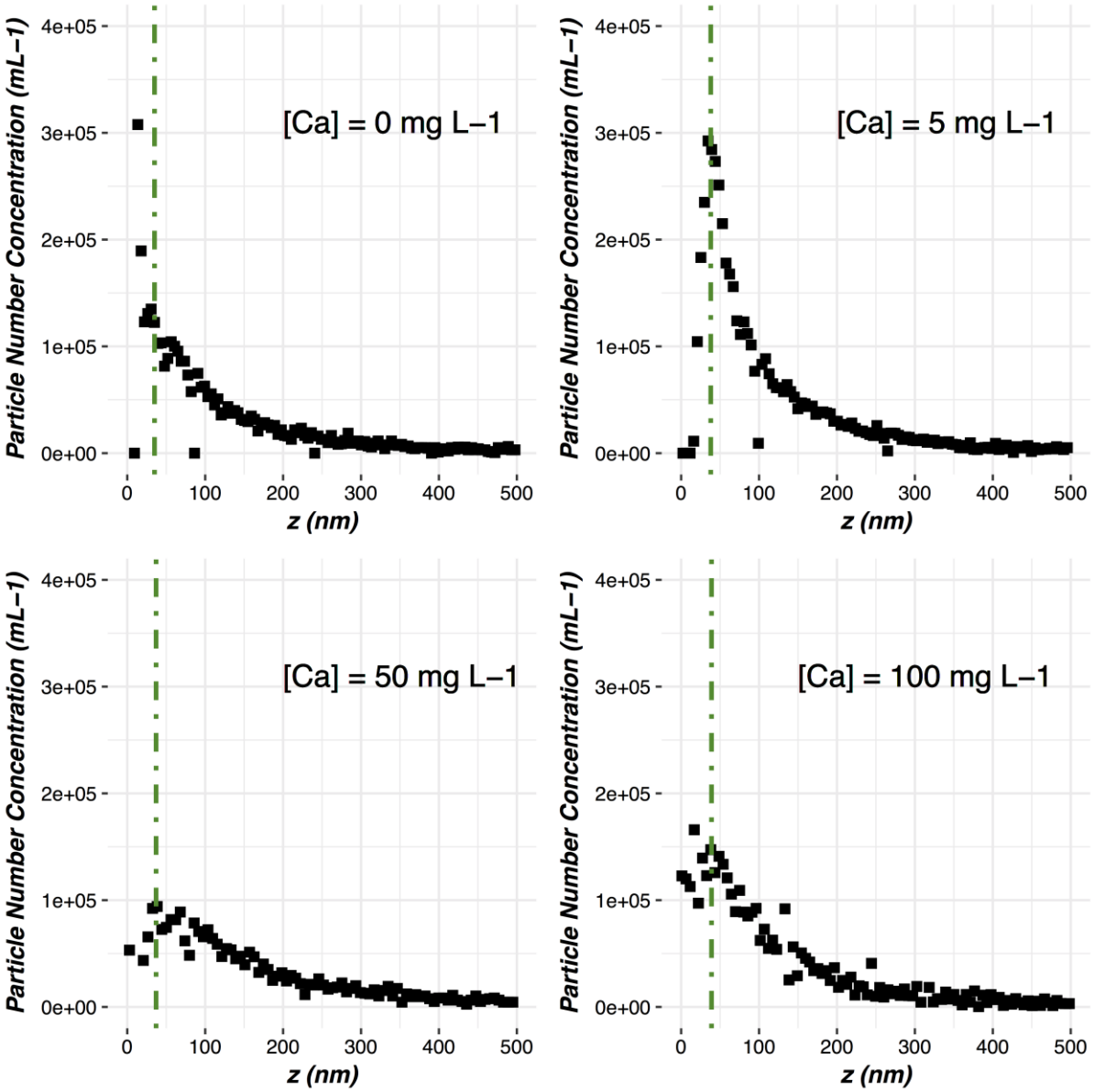

Figure 6. Graphs of particle number concentration (mL^{-1}) vs. 3rd dimension of the ellipsoid (nm) based on data measured with HR-ICP-MS. Squares represent the 3rd dimension size distribution of TiO_2 NM104 solutions in Ultrapure water (top left), 5 mg(Ca) L^{-1} (top right), 50 mg(Ca) L^{-1} (bottom left) and 100 mg(Ca) L^{-1} (bottom right). The green dotted line represents the 3rd dimension mode size ($z_{Deconvolution}$ in Table 3).